Stochastic Environmental Research and Risk Assessment 13 (1999) 161–182 © Springer-Verlag 1999

Impact of the simulation algorithm, magnitude of ergodic fluctuations and number of realizations on the spaces of uncertainty of flow properties

P. Goovaerts

Abstract. Geostatistical simulation algorithms are routinely used to generate conditional realizations of the spatial distribution of petrophysical properties, which are then fed into complex transfer functions, e.g. a flow simulator, to yield a distribution of responses, such as the time to recover a given proportion of the oil. This latter distribution, often referred to as the space of uncertainty, cannot be defined analytically because of the complexity (non-linearity) of transfer functions, but it can be characterized algorithmically through the generation of many realizations. This paper compares the space of uncertainty generated by four of the most commonly used algorithms: sequential Gaussian simulation, sequential indicator simulation, *p*-field simulation and simulated annealing. Conditional to 80 sample permeability values randomly drawn from an exhaustive 40×40 image, 100 realizations of the spatial distribution of permeability values are generated using each algorithm and fed into a pressure solver and a flow simulator. Principal component analysis is used to display the sets of realizations into the joint space of uncertainty of the response variables (effective permeability, times to reach 5% and 95% water cuts and to recover 10% and 50% of the oil). The attenuation of ergodic fluctuations through a rank-preserving transform of permeability values reduces substantially the extent of the space of uncertainty for sequential indicator simulation and *p*-field simulation, while improving the prediction of the response variable by the mean of the output distribution. Differences between simulation algorithms are the most pronounced for long-term responses (95% water cut and 50% oil recovery), with sequential Gaussian simulation yielding the most accurate prediction. In this example, utilizing more than 20 realizations generally increases only slightly the size of the space of uncertainty.

Key words: stochastic simulation, space of uncertainty, flow simulator, ergodic fluctuations.

Introduction

Reservoir management requires detailed 3D models of lithofacies, porosity, and permeability. Geostatistical simulation is increasingly used to build such models conditionally to a variety of information, such as seimic survey, core porosity or

P. Goovaerts
Department of Civil and Environmental Engineering,
The University of Michigan,
EWRE Bldg, Room 117,
Ann Arbor, MI 48109-2125
Phone: (734) 936-0141, Fax: (734) 763-2275,
e-mail: goovaert@engin.umich.edu

permeability, well logs, ... The advantage of stochastic simulation over interpolation (kriging) is that it allows reproduction of statistics (histogram, semivariogram, scattergram) inferred from the data, hence the model or realization looks more "realistic" than a smooth estimated map. Also, one can generate multiple realizations that all reasonably match the same sample statistics and exactly identify the conditioning data. The set of alternative realizations provides a visual and quantitative measure (actually a model) of *spatial uncertainty*. Spatial features, such as specific strings of large permeability values, are deemed certain if seen on most of the simulated maps. Conversely, a feature is deemed uncertain if seen only on a few simulated maps.

Simulation can be accomplished using a growing variety of techniques which differ in the underlying random function model (multiGaussian or non parametric), the amount and type of information that can be accounted for, and the computer requirements (Gotway and Rutherford, 1994; Myers, 1996; Srivastava, 1996; Deutsch and Journel, 1998). There is no simulation algorithm that is best for all cases but rather a toolbox of alternative algorithms from which to choose or to build the algorithm best suited for the problem at hand (Gómez-Hernández, 1997). According to Srivastava (1996), geostatistical realizations can be used for three main purposes:

1. To assess the impact of uncertainty. Petroleum engineers who are responsible for forecasting the future production of a reservoir seek "pessimistic" and "optimistic" models so that decisions are flexible enough to handle the uncertainty prevailing at the site.
2. To reproduce spatial variation. The objective is here to generate a single map that reproduces the pattern of spatial variability inferred from the data, and this realization is thus seen as a better alternative to a single smooth estimated map.
3. To perform Monte-Carlo risk analysis. Hundreds of alternate models are generated and processed to produce a distribution of possible values for some critical engineering parameters. For example, the processing of a set of permeability maps through a flow simulator allows the derivation of a set of possible values for the time to recover 10% of the oil. The distribution (histogram) of the response values corresponding to the set of input realizations provides a measure of response uncertainty resulting from our imperfect knowledge of the distribution in space of the petrophysical properties.

The first type of application requires the generation of many realizations, and so the computational time is of primary concern. In contrast, for the generation of a single simulated map the priority should be given to a very flexible algorithm, such as simulated annealing, that can accommodate very different kinds of information. Last, Monte-Carlo analysis requires the generation of many equiprobable realizations, hence the simulation algorithm should be chosen according to its computational speed and, more importantly, its ability to sample fairly the set of possible outcomes, which is referred to as the space of uncertainty.

The concept of space of uncertainty, and the associated issue of equiprobability of realizations, has triggered lively discussions in the recent geostatistical literature (Myers, 1994, 1996; Journel, 1994, 1997; Rossi, 1994; Srivastava, 1994, 1996, 1997). Some believe that the space of uncertainty must be theoretically defined outside the use of a particular algorithm. Others state that the space of uncertainty can only be defined through the algorithm and consists of all possible realizations that could be generated by the algorithm. This view is particularly

suited to the space of uncertainty of responses or output values which cannot be defined analytically because of the complexity (non-linearity) of transfer functions, such as flow simulators. In the latter case, the term of algorithmically-defined space of uncertainty is used (Deutsch, 1994).

There is currently no theory that allows us to determine if the set of all possible outcomes is fairly sampled. According to Journel (1997), for a given simulation algorithm, equiprobability is ensured as soon as each of the realizations is fully triggered by one random seed drawn from a uniform distribution. The problem is that each algorithm will sample a different subset of solutions. As speculated by Srivastava (1994), specific outcomes generated by one algorithm could not be generated by another, hence the choice of a simulation algorithm might be a key step in reservoir characterization.

Users are now aware that simulation algorithms that capitalize on the congenial properties of the multiGaussian RF model tend to generate realizations that show no significant correlation of extreme values (Journel and Alabert, 1988; Gómez-Hernández and Wen, 1994). Algorithms such as sequential Gaussian simulation are thus inappropriate for applications where it is critical to reproduce the connectivity of low or high values, e.g. strings of high permeability values may form flow paths. Journel and Deutsch (1993) have also shown that the property of maximum entropy of the multiGaussian RF model may lead to over-optimistic (narrow) assessment of uncertainty about response values, such as effective permeability or time to reach a 90% water cut. Deutsch and Journel (1992) compared the spaces of uncertainty generated by three simulation algorithms: sequential indicator simulation (sis), sequential Gaussian simulation (sGs), and simulated annealing (SA). In their study, all algorithms used the same information, that is the normal score semivariogram model, and the realizations were unconditional. Regardless of the response variable (time to recover 50% of the oil, times to achieve 5% and 95% water cut), the three algorithms generated comparable spaces, although the response distribution was slighly wider for simulated annealing. A rank-preserving transform of sis and sGs realizations reduced ergodic fluctuations in the histogram of permeability values, leading to narrower distributions of response values.

The characterization of the space of uncertainty is rendered difficult by the fact that only a limited number of realizations is usually generated. A frequent and still open question relates to the number of realizations needed to characterize this space. Rossi (1994) investigated the impact of the number of realizations on the average reproduction of univariate and bivariate statistics, such as the mean, variance and semivariogram of simulated values. He found that statistics reproduction improves with increasing number of realizations, and that Gaussian simulation algorithms allow one to reach "asymptotes" faster than indicator-based ones. This number also depends on the ratio of the semivariogram range to the size of the simulated domain: fewer realizations are needed for small range values. These results, however, simply reflect ergodic fluctuations of simulated realizations (Deutsch and Journel, 1998, p. 129) and bring little insight into the size of the space of uncertainty of response values, which is one main concern for reservoir management.

In summary, contrasting with the increasing use of stochastic simulation in risk analysis, it appears that little attention has been paid to the definition of the space of uncertainty, and related issues such as the equiprobability of realizations, the equivalence of spaces of uncertainty generated by different algorithms, and the number of realizations required to sample this space. To quote Myers (1996),

"Underlying this diversity of algorithms was an implicit but never stated assumption that there was some form of equivalence and hence the difference was only computational... Neither of these implicit assumptions has really been tested or even considered, most users do not use multiple algorithms and make comparisons nor do they generate multiple finite sets of realizations to compare between the sets."

This paper brings new insight into the comparison of spaces of uncertainty by considering the increasingly used *p*-field simulation algorithm in addition to the well-known sequential indicator and Gaussian simulation, and simulated annealing. Instead of looking at the space of uncertainty of each flow characteristic taken separately, I propose to use principal component analysis to display the set of realizations into the space defined by all characteristics together, which amounts at looking at the multivariate space of uncertainty. Last, the impact of the number of realizations and magnitude of ergodic fluctuations on the extent of the space of uncertainty is investigated. The comparative study is based on a petroleum example, yet the same methodology can be applied to a variety of problems, such as the modeling of groundwater flow or solute transport.

Stochastic simulation

This section briefly reviews the main features of the simulation algorithms used in the comparative study. A thorough presentation of these algorithms is available in textbooks such as Goovaerts (1997, p. 376–424) or Deutsch and Journel (1998, p. 119–197). Many other techniques have been developed for the simulation of spatial phenomena, e.g. see Ripley (1981) or Christakos (1992, p. 294–336), but the focus is here on major algorithms that are used in geostatistics, mainly because of their flexibility and ease of generating conditional realizations.

Sequential Gaussian and indicator simulation

Consider the simulation of the continuous attribute z at N grid nodes $\mathbf{u}'_j$ conditional to the data set $\{z(\mathbf{u}_\alpha),\ \alpha = 1, \ldots, n\}$. Sequential simulation (Journel and Alabert, 1988; Isaaks, 1990; Gómez-Hernández and Srivastava, 1990) amounts to modeling the conditional cumulative distribution function (ccdf) $F(\mathbf{u}'_j; z|(n)) = \text{Prob}\{Z(\mathbf{u}'_j) \leq z|(n)\}$, then sampling it at each of the grid nodes visited along a random sequence. To ensure reproduction of the z-semivariogram model, each ccdf is made conditional not only to the original n data but also to all values simulated at previously visited locations. Other realizations $\{z^{(l')}(\mathbf{u}'_j),\ j = 1, \ldots, N\}$, $l' \neq l$, are obtained by repeating the entire sequential drawing process.

Two major classes of sequential simulation algorithms can be distinguished, depending on whether the series of conditional cdfs are determined using the multiGaussian or the indicator formalism. Sequential Gaussian simulation (sGs) typically involves a prior transform of the z-data into y-data with a standard normal histogram, which is referred to as a normal score transform. The simulation is then performed in the normal space, and the simulated normal scores are back-transformed in order to identify the original z-histogram $\widehat{F}(z)$. Note that because the histogram of simulated y-values is never exactly normal, the histogram of back-transformed simulated values may slightly deviate from the target histogram $\widehat{F}(z)$.

Sequential indicator simulation (sis) starts with the transform of each z-datum into a vector of indicator data defined for a series of K threshold values dis-

cretizing the range of variation of z. In this paper, 5 threshold values corresponding to the 1st, 3rd, 5th, 7th, and 9th deciles of the sample cdf $\widehat{F}(z)$ were used. The resolution of the discrete ccdf was increased by performing a linear interpolation between tabulated bounds provided by the sample cdf (Deutsch and Journel, 1998, p. 136). Unlike sequential Gaussian simulation, no systematic back-transform allows reproduction of a target histogram by simulated values. However, the realization can be post-processed using the algorithm developed by Journel and Xu (1994) to improve reproduction of the target cdf while still honoring the conditioning data and without significant modification of the spatial correlation patterns in the original realization.

p-field simulation

The *p*-field approach (Srivastava, 1992; Froidevaux, 1993) also requires the sampling of successive ccdfs. However, unlike the sequential approach, all ccdfs are conditioned only to the original n data. Reproduction of the z-semivariogram model is here approximated by imposing an autocorrelation pattern on the probability values used for sampling these ccdfs (Journel, 1995). This approach allows the rapid generation of a large number of realizations. In this paper, the ccdfs were modeled using an indicator approach, which allows one to account for class-specific patterns of spatial continuity through different indicator semivariogram models. Like sequential indicator simulation, better reproduction of the target histogram can be ensured by a post-processing of the realizations using Journel and Xu's algorithm.

Simulated annealing

Unlike the previous simulation algorithms, in simulated annealing (SA) the creation of a stochastic image is formulated as an optimization problem without any specific reference to a RF model (Geman and Geman, 1984; Ripley, 1987; Farmer, 1988; Deutsch and Journel, 1992; Deutsch and Cockerham, 1994; Goovaerts, 1998a). The basic idea is to perturb an initial (seed) image gradually so as to match target constraints, such as reproduction of the z-semivariogram model. Simulated annealing is a very flexible approach that can produce realizations that honor many different kinds of information, but it can become very time consuming if numerous and conflicting constraints are considered.

In this paper, initial random images, which reproduce the z-histogram, were perturbed by swapping z-values at any two locations chosen at random. The target constraint was the reproduction of indicator semivariograms, and the corresponding objective function was lowered using a default annealing schedule (Deutsch and Cockerham, 1994). Because the perturbation mechanism does not change the target histogram of the initial image, the final realization reproduces the target histogram without the help of any back-transform or post-processing of simulated values.

Case study

Figure 1 (left top graph) shows the spatial distribution of 40×40 minipermeater measurements taken from a 2 by 2 foot vertical slab of a Berea sandstone, and hereafter considered as the reference image (Giordano et al., 1985). Eighty locations were drawn at random and form our sample data set which is considered as the sole information available for the reconstruction of the whole image using different simulation algorithms. Figure 1 (right column) shows that the exhaustive and sample statistics deviate somewhat.

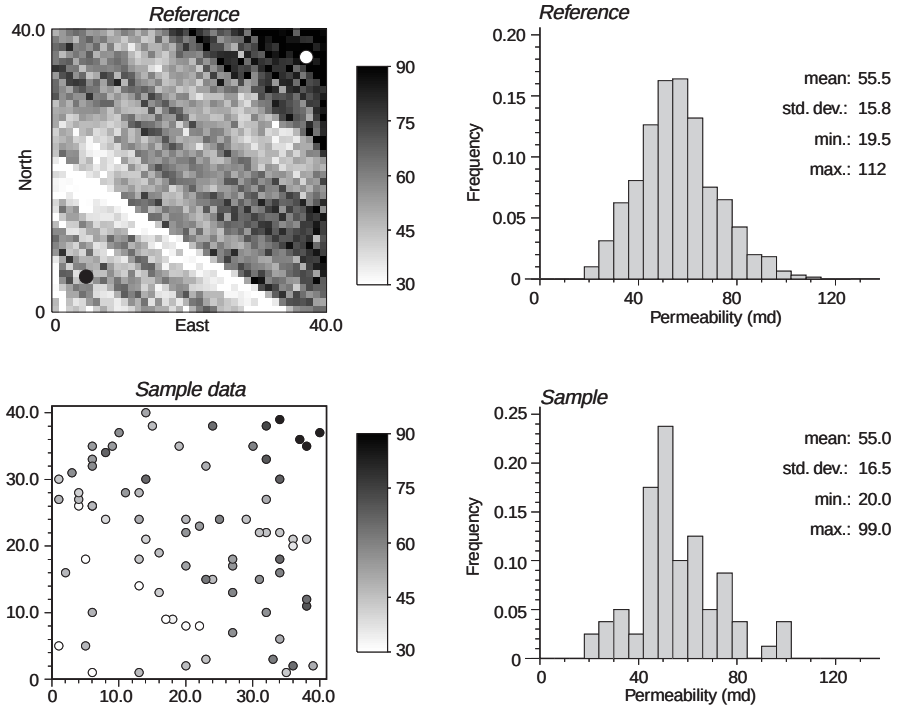

Fig. 1. Reference permeability map with the locations of the producer (open circle) and injector (black dot) for flow simulation. The information available consists of 80 randomly drawn values and the sample histogram

Indicator semivariograms were computed for five threshold values corresponding to the 1st, 3rd, 5th, 7th, and 9th deciles of the sample distribution of 80 permeability values, see Fig. 2. For all thresholds, a geometric anisotropy model was fitted with a smaller range in the direction of azimuth 35°, that is the direction perpendicular to the banding of low values in Fig. 1. The anisotropy ratio drops from 5 to 2 as the threshold value increases, which indicates that the anisotropy is less pronounced for high permeability values. A similar anisotropic model is fitted to the normal score semivariogram displayed in Fig. 2 (right bottom graph).

Permeability maps

One hundred realizations of permeability values were generated using each of the four simulation algorithms. The first realizations are shown in Fig. 3. At each grid node $\mathbf{u}'_j$, the ccdf $F(\mathbf{u}'_j; z|(n))$ is numerically approximated by the cumulative distribution of the 100 values simulated there:

$$\widehat{F}(\mathbf{u}'_j; z|(n)) = \widehat{\text{Prob}}\{Z(\mathbf{u}'_j) \leq z|(n)\} = \frac{1}{L}\sum_{l=1}^{L} i^{(l)}(\mathbf{u}'_j; z) \quad j = 1, \ldots, N \tag{1}$$

with $i^{(l)}(\mathbf{u}'_j; z) = 1$ if $z^{(l)}(\mathbf{u}'_j) \leq z$, and zero otherwise. For example, Fig. 4 shows the histograms of 100 permeability values generated using sequential indicator simulation at the left and right bottom corners of the simulation grid.

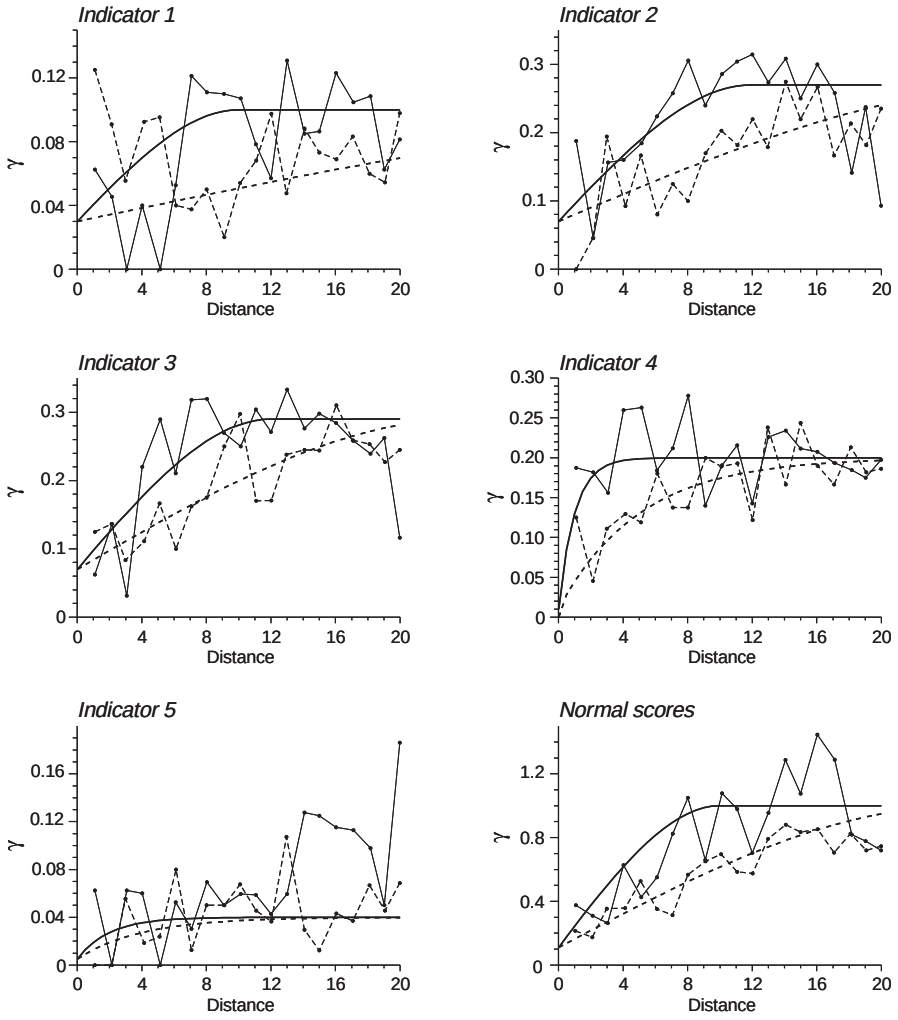

Fig. 2. Experimental semivariograms computed in two directions (— : 35°, – – : 125°) for indicator and normal score transforms of the 80 permeability values of Fig. 1. In each case, a geometric anisotropy model was fitted, with a larger range in the 125° direction

Deutsch (1997) states that a probability distribution is accurate if the fraction of true values falling in the symmetric p-probability interval (PI) exceeds p for all $p \in [0, 1]$. For a given probability p, the upper and lower bounds of the symmetric p-PI are $(1 - p)/2$ and $(1 + p)/2$ quantiles, respectively. Because the true values $z(\mathbf{u}'_j)$ are here known, these fractions are readily computed as:

$$\overline{\xi(p)} = \frac{1}{N} \sum_{j=1}^{N} \xi(\mathbf{u}'_j; p) \;\forall\; p \in [0, 1] \tag{2}$$

with:

$$\xi(\mathbf{u}'_j; p) = \begin{cases} 1 & \text{if } \widehat{F}^{-1}(\mathbf{u}'_j;\ (1-p)/2) < z(\mathbf{u}'_j) \leq \widehat{F}^{-1}(\mathbf{u}'_j; (1+p)/2) \\ 0 & \text{otherwise} \end{cases} \tag{3}$$

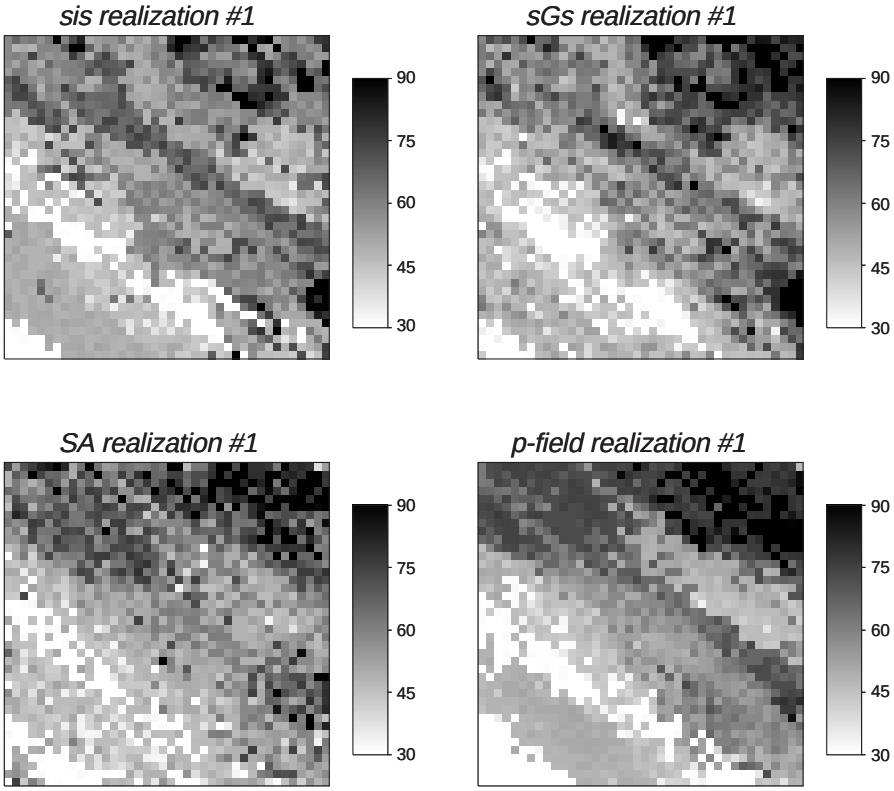

Fig. 3. First realization of the spatial distribution of permeability values generated by each of the four simulation algorithms

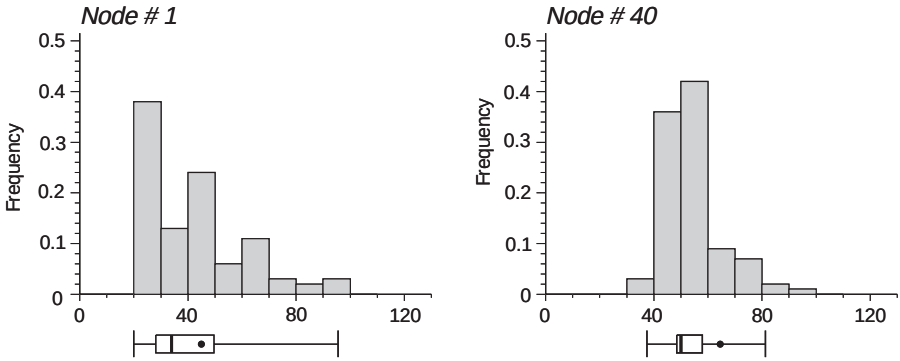

Fig. 4. Histograms of 100 simulated values generated using sequential indicator simulation at 2 grid nodes. The black dot in the box plot below each histogram is the true permeability value. Five vertical lines are the 0.025 quantile, lower quartile, median, upper quartile, and 0.975 quantile of the distribution

The accuracy of a probabilistic model can be visually assessed by plotting the fractions (2) versus the set of probabilities p. The so-called accuracy plot (Deutsch, 1997) is depicted at Fig. 5 for each simulation algorithm. For all four algorithms, all the points fall below the 45° line, i.e. $\overline{\xi(p)} < p$ for all p, which

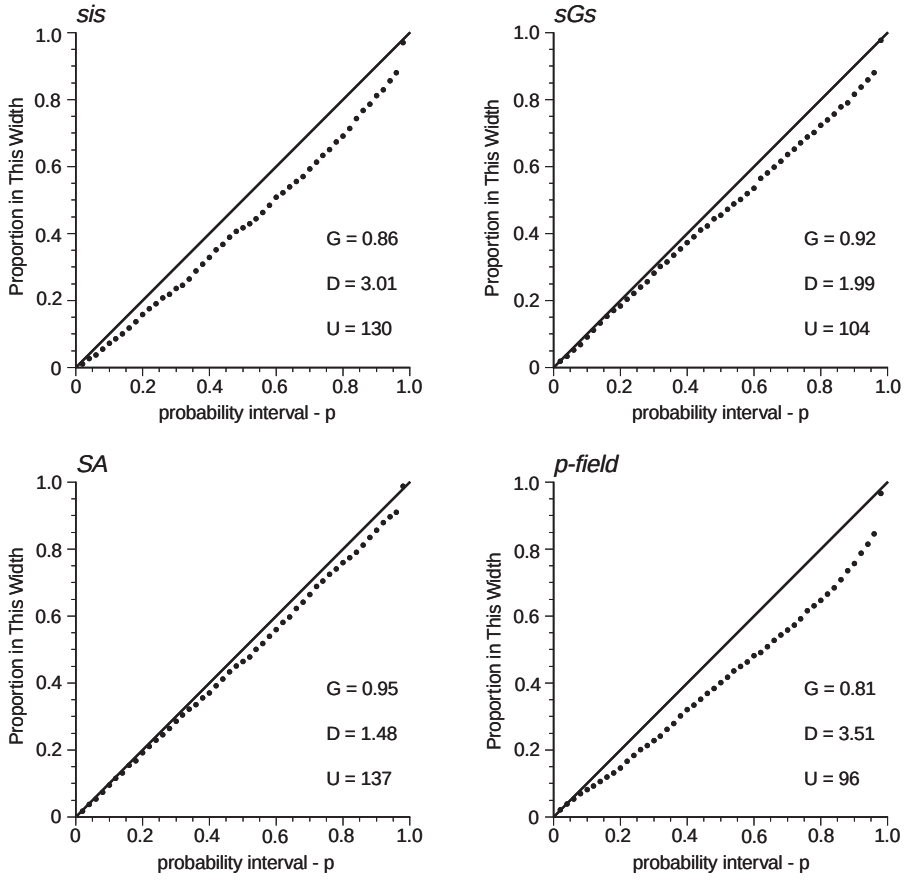

Fig. 5. Accuracy plots and some summary characteristics for the four simulation algorithms

indicates that the probabilistic models are inaccurate. For example, the 0.5 probability intervals derived from sequential indicator realizations only contain 42% of the true values.

Although all models are inaccurate, departures from the 45° line are small for simulated annealing (SA) and sequential Gaussian simulation (sGs), and a measure of this closeness is the goodness statistic $G \in [0,1]$ defined as (Deutsch, 1997):

$$G = 1 - \int_0^1 [3a(p) - 2]\ [\overline{\xi(p)} - p]\ dp \tag{4}$$

where the indicator function $a(p)$ is defined as:

$$a(p) = \begin{cases} 1 & \text{if } \overline{\xi(p)} \geq p \\ 0 & \text{otherwise} \end{cases} \tag{5}$$

Twice more importance is given to deviations when $\overline{\xi}(p) < p$ (inaccurate case): the weight $|3a(p) - 2| = 2$ instead of 1 for the accurate case, that is the case where the fraction of true values falling into the p-probability interval is larger than

expected. Smallest (poorest) G values are obtained for sequential indicator simulation (sis) and p-field simulation, i.e. the two algorithms that do not impose reproduction of the histogram either explicitly like simulated annealing or through a back-transform like sequential Gaussian simulation. The average magnitude of deviations from the reference histogram is measured by the statistic D defined as:

$$D = \frac{1}{KL} \sum_{l=1}^{L} \sum_{k=1}^{K} |q_k - q_k^{(l)}| \tag{6}$$

where $q_k^{(l)} = F_{(l)}^{-1}(p_k)$ is the p_k-quantile of the histogram of the lth realization, and q_k is the corresponding quantile of the reference histogram of Fig. 1. Note that simulated annealing and sequential Gaussian simulation impose reproduction of the sample histogram which deviates from the exhaustive (reference) histogram, hence the statistics D is not close to zero for these two algorithms, see Fig. 5. Also, the goodness statistics increases when the magnitude of ergodic fluctuations, as measured by statistics D, decreases. To allow a fair comparison between algorithms, the realizations generated by sequential indicator simulation and p-field simulation were transformed using the rank-preserving algorithm developed by Journel and Xu (1994). Again, the reproduction of the sample histogram, which is the only one available in practice, was imposed. Such a transform reduces the magnitude of ergodic fluctuations: $D = 1.64$ (initial value 3.01) and $D = 1.79$ (initial value 3.51) for sequential indicator simulation and p-field simulation, respectively. Whereas the goodness statistic increases from 0.86 to 0.90 for the post-processed sis realizations, the transform has no impact on the goodness of the probabilistic model generated by the p-field simulation.

Another characteristic of the probabilistic models is the spread of the local distributions of 100 simulated values which is a measure of local uncertainty. The statistic U given in Fig. 5 is the average variance of the $N = 1600$ distributions of simulated values, one per grid node:

$$U = \frac{1}{N} \sum_{j=1}^{N} \widehat{\sigma}^2(\mathbf{u}'_j) \tag{7}$$

with:

$$\widehat{\sigma}^2(\mathbf{u}'_j) = \frac{1}{L-1} \sum_{l=1}^{L} \left[z^{(l)}(\mathbf{u}'_j) - z_E^*(\mathbf{u}'_j) \right]^2$$

where the E-type estimate $z_E^*(\mathbf{u}'_j)$ is the arithmetic average of the 100 simulated values at $\mathbf{u}'_j$, that is the mean of the local distribution. Statistics U should be as small as possible while preserving accuracy and precision. The local uncertainty is largest for simulated annealing ($U = 137$) and smallest for p-field simulation ($U = 96$), which contrasts with the existence of smaller ergodic fluctuations for SA realizations. The large value of U for SA realizations is probably due to the swapping perturbation mechanism, which is much less constraining (i.e. more possible outcomes) than the sampling of a ccdf as performed for other simulation algorithms. An alternative to the swapping mechanism would be to select randomly a location and replace the current value by a new value randomly drawn

from the conditional cdf which can be modeled prior to the simulation (Goovaerts, 1998b) or updated during the optimization process (Deutsch and Wen, 1998). In this way, we gain more control on the local distributions of simulated values. In particular, any prior or soft information could be incorporated in the modeling of local ccdfs to be sampled by simulated annealing, e.g. see Goovaerts (1997, p. 306–319).

Flow properties

The effective permeability of each realization was computed in both the E-W and N-S directions using the pressure solver *flowsim* (Deutsch and Journel, 1992). A waterflood simulator (Eclipse, 1991) was then applied to each realization using the injection/production pattern in Fig. 1; the flow is thus perpendicular to the diagonal banding of permeability values. The fractional flow of oil versus time was recorded, and four values were retrieved: the times to reach 5% and 95% water cut, and the times to recover 10% and 50% of the oil.

The space of uncertainty of flow characteristics is usually represented by the histogram of response values for each variable taken separately, i.e. 6 histograms in this case (2 effective permeabilities + 4 times). For example, Fig. 6 shows the histograms for the N-S effective permeability (left column) and the time to reach 5% water cut (right column). For both response variables, the spread of the distribution is largest for realizations generated using *p*-field simulation (largest output uncertainty). Simulated annealing yields a very narrow distribution of effective permeability values. The two sequential algorithms generate spaces of uncertainty of similar extent. In all cases, the 95% probability interval includes the true value that was derived from the reference image of Fig. 1 and is depicted by the black dot: $\overline{K}^{x}_{\text{eff}} = 53.1$ md, and the 5% water cut is reached at 2.56 time units. As long as the distribution is accurate, that is contains the true value, the narrowness (precision) of the distribution is highly desirable. Best results are thus provided by simulated annealing for effective permeability, whereas all algorithms perform similarly for 5% water cut.

To study how ergodic fluctuations in the reproduction of the permeability histogram affects the distribution of response values, the pressure solver and flow simulator were also applied to the sis and *p*-field realizations after transformation using the rank-preserving algorithm developed by Journel and Xu (1994). The comparison of histograms of Figs. 6 and 7 shows that the attenuation of ergodic fluctuations leads to narrower distributions of N-S effective permeability and time to reach 5% water cut. Table 1 shows this reduction to occur for all response variables: the standard deviation of output distributions has been reduced by an average of 60% for effective permeability and by a range of 25%–50% for other flow characteristics. Besides a reduction of output uncertainty, the attenuation of ergodic fluctuations improves the prediction of the true response value by the mean of the output distribution, see Table 2. The prediction error has been reduced by an average of 40% ! This reduction is mostly due to the similarity between the sample and reference histograms of Fig. 1. When too few data are available to infer reliable histograms, one should be cautious in imposing the strict reproduction of a target histogram which might be far from the true one and so leads to worse predictions. In this example, all simulation algorithms underestimate the effective permeability, leading to an overestimation of the times to reach the two water cuts or to recover proportions of the oil.

Simulated annealing provides the most precise and accurate prediction of effective permeability in that the corresponding output distribution has the smallest variance while its mean is the closest to the true value. Sequential Gaussian

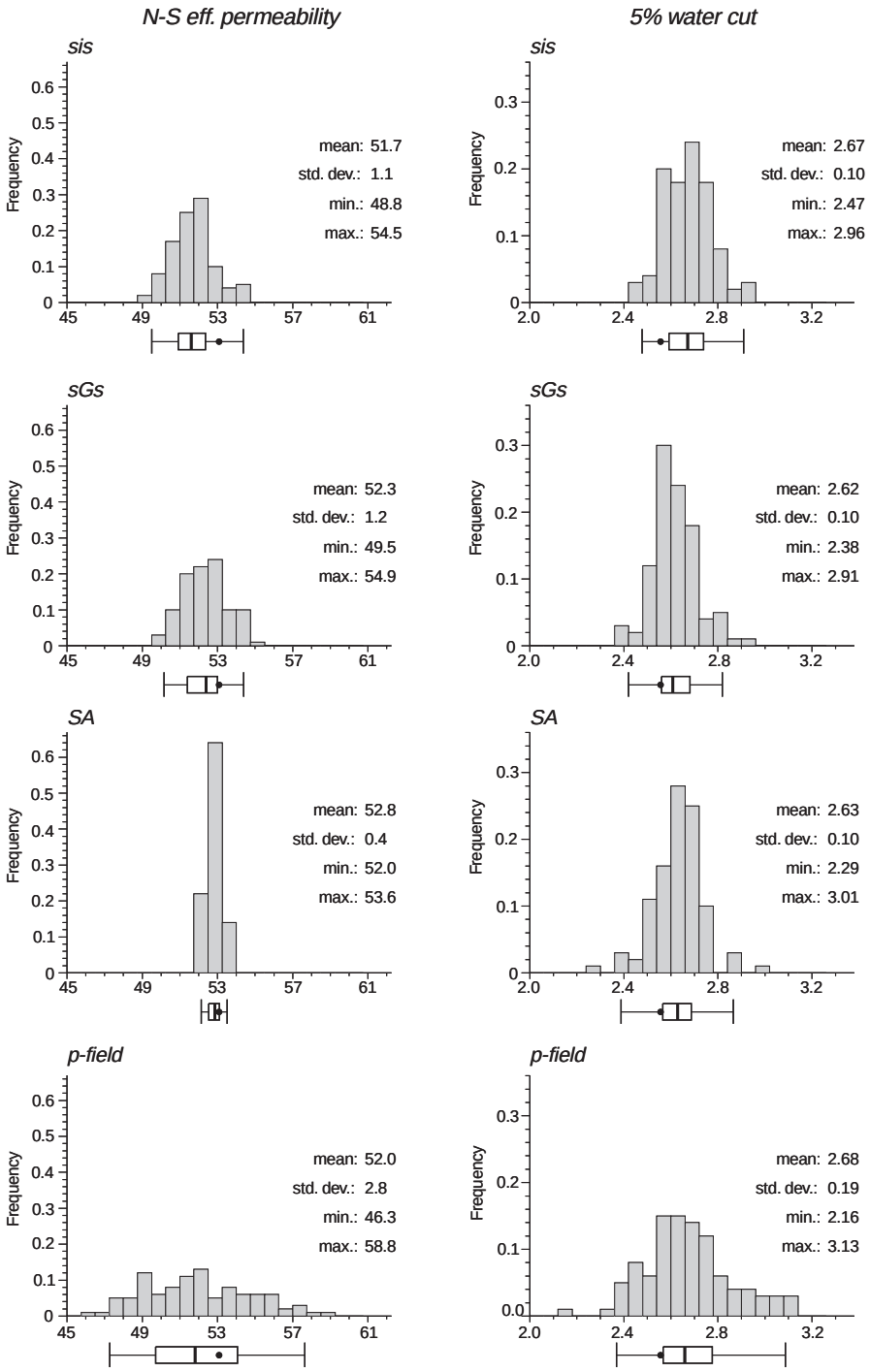

Fig. 6. Histograms of the N-S effective permeability (left column) and the time to reach 5% water cut (right column) assessed from 100 realizations generated by each simulation algorithm. The black dot in the box plot below each histogram is the true value obtained from the reference image of Fig. 1. Five vertical lines are the 0.025 quantile, lower quartile, median, upper quartile, and 0.975 quantile of the distribution

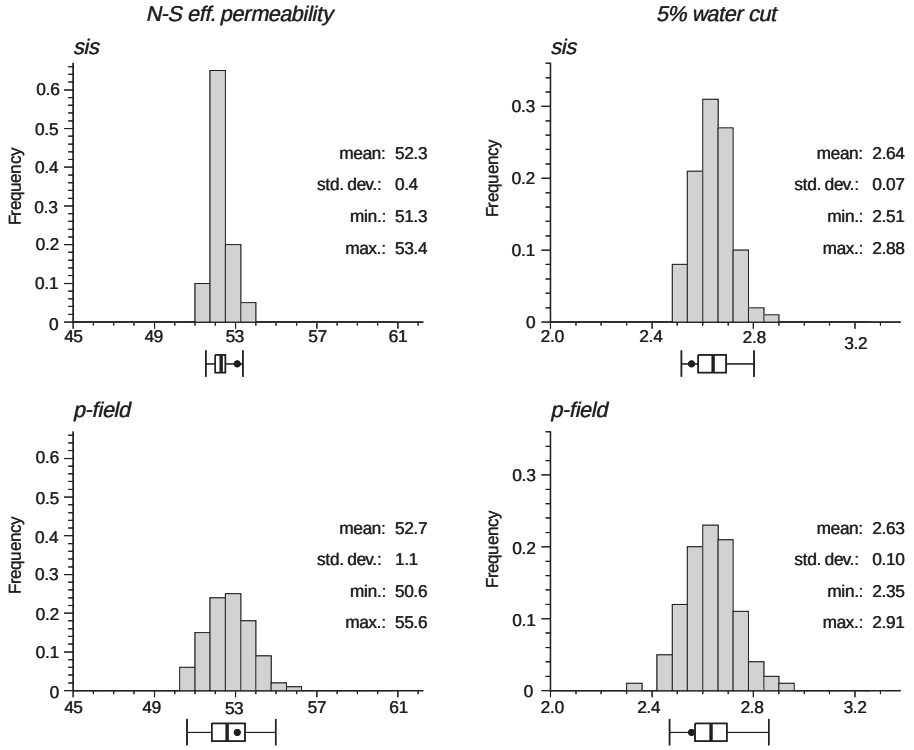

Fig. 7. Impact of the reduction of ergodic fluctuations (better reproduction of the histogram of permeability) on the output distribution of N-S effective permeability (left column) and time to reach 5% water cut (right column) for sequential indicator simulation and *p*-field simulation. Distributions are much narrower than the corresponding histograms of Fig. 5

simulation performs best for flow simulation results, which is surprising because the indicator semivariograms of Fig. 2 show the multiGaussian assumption to be violated for the Berea data set: the pattern of spatial correlation is not symmetric about the median since the anisotropy is more pronounced for low permeability values (Journel and Alabert, 1989).

Table 3 gives the coefficients of linear correlation between the 6 flow characteristics computed over all simulation algorithms (400 realizations). The N-S and

Table 1. Std. deviation of the output distribution for the 6 response variables: N-S effective permeability ($\overline{K}^{x}_{\text{eff}}$), E-W effective permeability ($\overline{K}^{y}_{\text{eff}}$), times to reach 5% ($Wc_1$) and 95% ($Wc_2$) water cut, and the times to recover 10% (Oil_1) and 50% (Oil_2) of the oil

	$\overline{K}^{x}_{\text{eff}}$	$\overline{K}^{y}_{\text{eff}}$	Wc_1	Wc_2	Oil_1	Oil_2
sis	1.14	1.22	0.10	0.64	0.04	0.35
sis transf.	0.43	0.50	0.07	0.48	0.03	0.27
sGs	1.17	1.18	0.10	0.51	0.04	0.29
p-field	2.80	3.04	0.19	1.05	0.08	0.62
p-field transf.	1.09	1.23	0.10	0.62	0.04	0.41
SA	0.37	0.37	0.10	0.70	0.04	0.39

Table 2. Difference between the mean of the output distribution and the true value for the 6 response variables

	$\overline{K}^{x}_{\text{eff}}$	$\overline{K}^{y}_{\text{eff}}$	Wc_1	Wc_2	Oil_1	Oil_2
sis	−1.42	−1.55	0.12	0.85	0.06	0.53
sis transf.	−0.80	−0.97	0.09	0.63	0.05	0.40
sGs	−0.80	−0.87	0.06	0.15	0.02	0.02
p-field	−1.08	−1.46	0.12	0.65	0.05	0.40
p-field transf.	−0.43	−0.84	0.08	0.40	0.03	0.22
SA	−0.26	−0.51	0.07	0.65	0.04	0.45

E-W effective permeabilities are highly correlated and, as expected, they are negatively correlated with the other response variables: the larger the effective permeability, the smaller the time to reach a given water cut or to recover a given proportion of the oil. Because of the correlation between response variables, their spaces of uncertainty should not be analyzed separately. Rather, one should look at the scatter of realizations in the six-dimensional space spanned by the six flow characteristics, that is characterize the multivariate space of uncertainty.

Principal component analysis (PCA) was used to display the 400 realizations in a subspace that can be visualized easily. The basic idea of PCA (Davis, 1986, p. 602) is to create new orthogonal variables, the principal components, as linear combinations of the original variables, i.e. the six response variables. The first few components generally account for most of the variance and so are the most informative. Figure 8 (middle graph) shows the scatter of the 400 realizations in the plane of the first two principal components which explain 94% of the total variance. For clarity two plots of 200 realizations have been drawn. The 2 principal components were rotated (Varimax rotation) to achieve a "simple structure", that is each response variable correlates mainly with one of the two principal components, which facilitates the interpretation of the components (Kaiser, 1958; Goovaerts, 1993). The correlations between response variables and principal components are usually displayed using a circle of correlation, see Fig. 8 (top graph). The coordinates of each variable on that circle are but their correlations with each of the first two components. The closer the variable to the perimeter of the circle, the larger its correlation with the principal components. The first factor depends essentially on flow simulation results, whereas the second factor represents mainly the E-W and N-S effective permeabilities. This grouping reflects the correlation structure detected in Table 3.

The two sequential algorithms generate spaces of uncertainty with substantial overlap; the scatter of realizations is larger for sequential indicator simulation which also leads to longer times for water cut and oil recovery (larger values of the

Table 3. Matrix of linear correlation coefficients between the 6 response variables

	$\overline{K}^{x}_{\text{eff}}$	$\overline{K}^{y}_{\text{eff}}$	Wc_1	Wc_2	Oil_1	Oil_2
$\overline{K}^{x}_{\text{eff}}$	1.00					
$\overline{K}^{y}_{\text{eff}}$	0.95	1.00				
Wc_1	−0.61	−0.59	1.00			
Wc_2	−0.51	−0.50	0.84	1.00		
Oil_1	−0.60	−0.58	0.90	0.98	1.00	
Oil_2	−0.44	−0.45	0.64	0.94	0.90	1.00

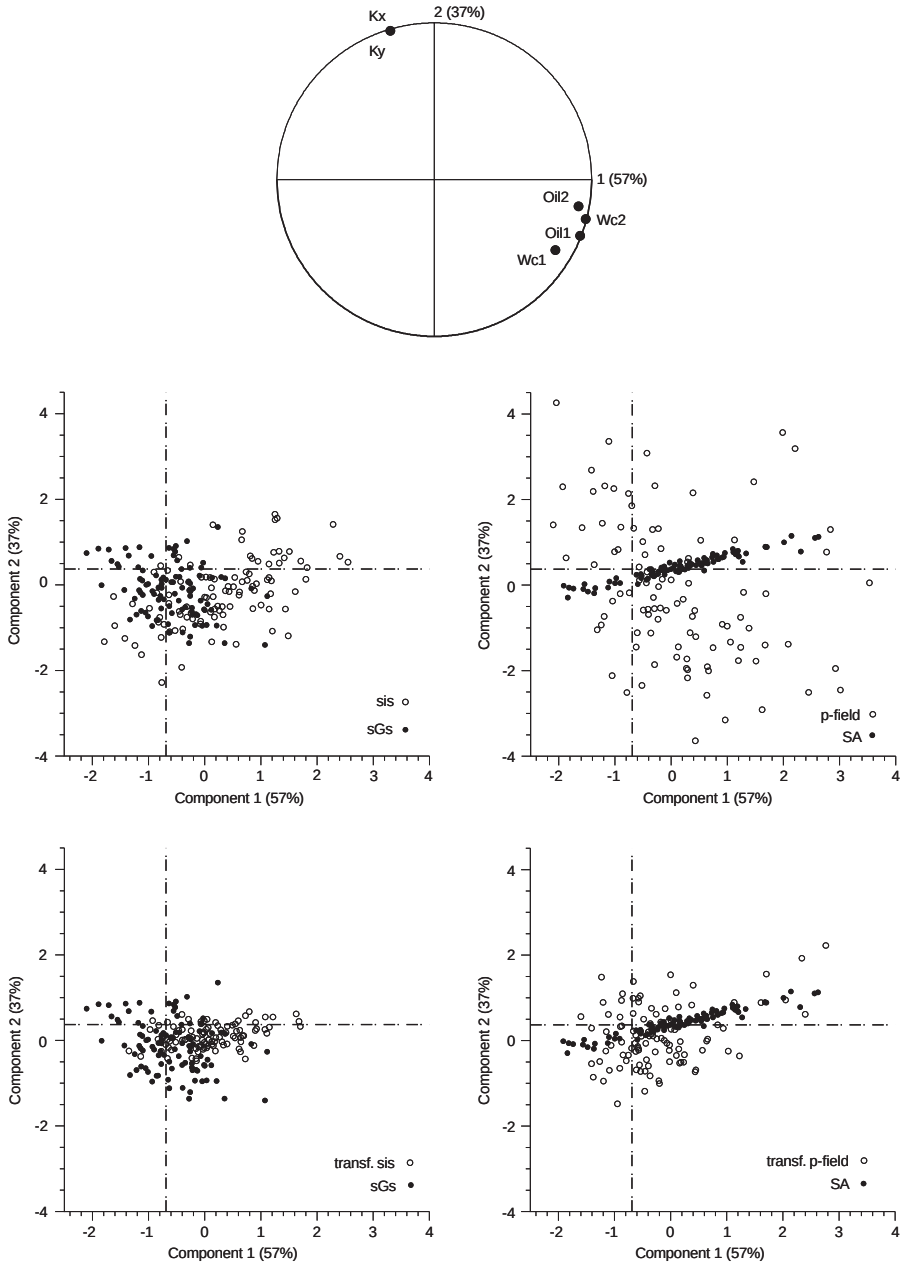

Fig. 8. Scatter of the 400 realizations in the plane defined by the first two rotated principal components of the correlation matrix of six flow properties. Bottom graphs show the impact of the reduction of ergodic fluctuations on the space of uncertainty of *p*-field and sequential indicator simulation. The circle of correlation (top graph) depicts the correlation between each of the flow characteristics and the two principal components

first component). The lowering of ergodic fluctuations narrows substantially the space of uncertainty for sis realizations and reduces slightly its overlap with the sGs space (Fig. 8, left bottom graph). Untransformed *p*-field realizations yield the largest space of uncertainty, whereas the space depicted by SA realiza-

tions is narrow along the vertical axis because of the similarity of effective permeability values, recall Fig. 5 (left column). The dispersion of SA realizations along the horizontal axis reflects the larger variance of flow simulation results, this is similar to what is observed for other algorithms. Like sequential indicator simulation, the transformation of p-field realizations scales down the space of uncertainty which still includes most of the three other spaces.

Another important characteristic of the space of uncertainty is whether it contains the true response values, which defines its accuracy. Reference values for the 6 response variables were obtained by applying the pressure solver and flow simulator to the reference image of Fig. 1. These values were combined to derive the true values for the first two principal components, see vertical and horizontal dashed lines in Fig. 8. For each component taken separately, the four spaces of uncertainty $\mathscr{S}_k$ are accurate in that they contain the true response values R_i, that is:

$$\text{Prob}\{R_i \in \mathscr{S}_k\} > 0 \quad i = 1,2 \; k = 1,4 \tag{8}$$

However, when considering the two components jointly, the confined space generated by simulated annealing, $\mathscr{S}_3$, does not contain the pair of true values which corresponds to the intersection of the two dashed lines:

$$\text{Prob}\{(R_1, R_2) \in \mathscr{S}_3\} = 0 \tag{9}$$

Had the response variables been uncorrelated, the multivariate spaces of uncertainty would have been circular, hence the accuracy for each variable taken separately will entail the accuracy for the joint set of response variables, that is the joint probability of containing the pair of true values would be the product of marginal probabilities:

$$\text{Prob}\{(R_1, R_2) \in \mathscr{S}_3\} = \text{Prob}\{R_1 \in \mathscr{S}_3\} \cdot \text{Prob}\{R_2 \in \mathscr{S}_3\} > 0 \tag{10}$$

In presence of correlation between response variables, it is thus informative to look at the joint space of uncertainty in addition to considering each variable separately.

Impact of the number of realizations

The generation of multiple realizations and their post-processing through transfer functions are computationally expensive, and it is worth investigating the impact of the number of realizations on the space of uncertainty of response values. For each simulation algorithm and response variable, the processing of the 100 realizations through a flow simulator or pressure solver yielded a set of 100 output values; recall Fig. 5. This set was randomly sampled to create 100 subsets of two values. Such a random sampling of the initial set of 100 values was repeated for increasing subset sizes: 3, 4, ... 100 values. Note that a value can be included only once in a subset (sampling without replacement). Thus, this resampling results in 100 subsets for each of the 99 possible sizes. For each subset, the following statistics were computed: mean, variance, minimum and maximum response values. These statistics were used to study the impact of the number of realizations (i.e. size of subset) on the following quantities:

- the standard deviation of the set of response values; the standard deviations of the 100 subsets were averaged for each size.

- the absolute deviation between the mean of the output distribution and the true value; prediction errors were computed for each subset and averaged.
- the upper and lower bounds of the space of uncertainty; these were identified with the average minimum and maximum response values over the 100 subsets.

Figure 9 (left column) shows that the standard deviation of the output distribution drastically increases when the first realizations are generated but, beyond 10 realizations, the rate of increase reduces because of the redundancy between conditional realizations. For 100 realizations, one retrieves the standard deviations listed in Table 1. Sequential indicator simulation consistently yields narrow output distributions, whereas simulated annealing produces the narrowest distribution for effective permeability but the largest one for the times to reach 5% and 95% water cuts.

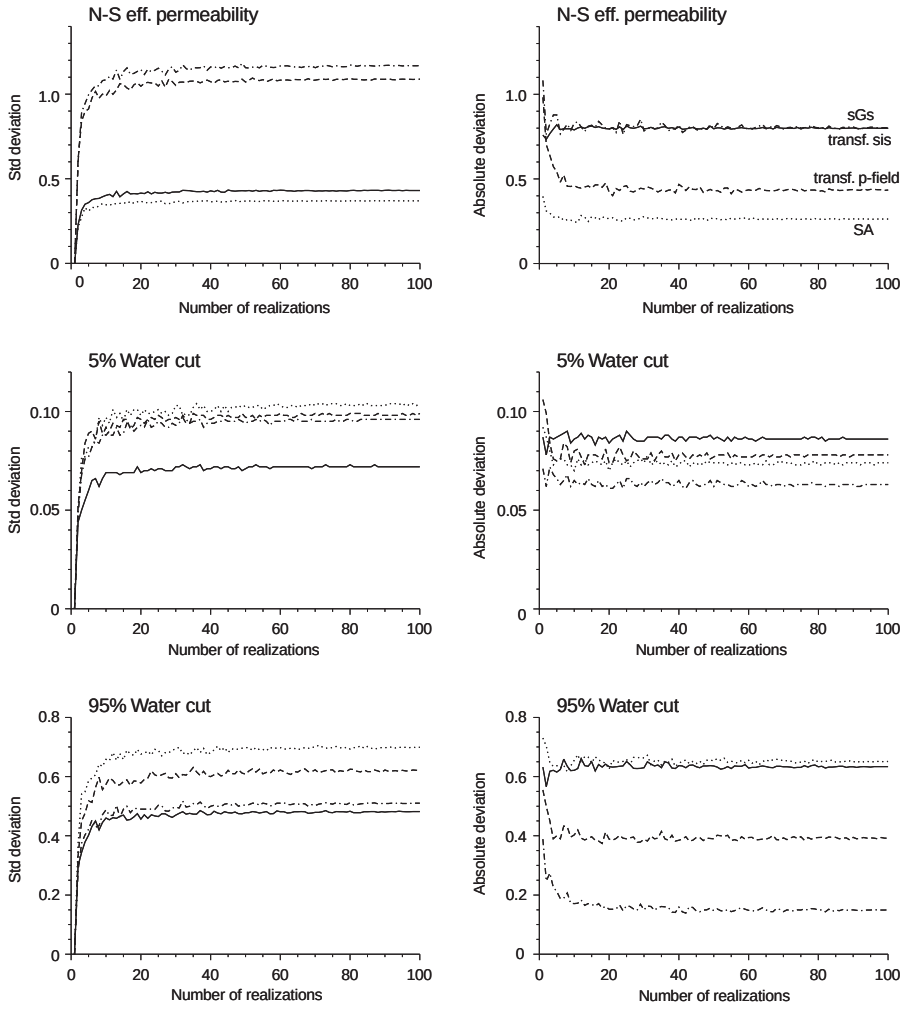

Fig. 9. Impact of the number of generated realizations on the standard deviation of the response distribution (left column) and on the absolute difference between the mean of this distribution and the true value derived from the reference image of Fig. 1 (right column). Best if both statistics are small. The algorithms are: — (transf. sis), - · - (sGs), - - (transf. *p*-field), · · · (SA)

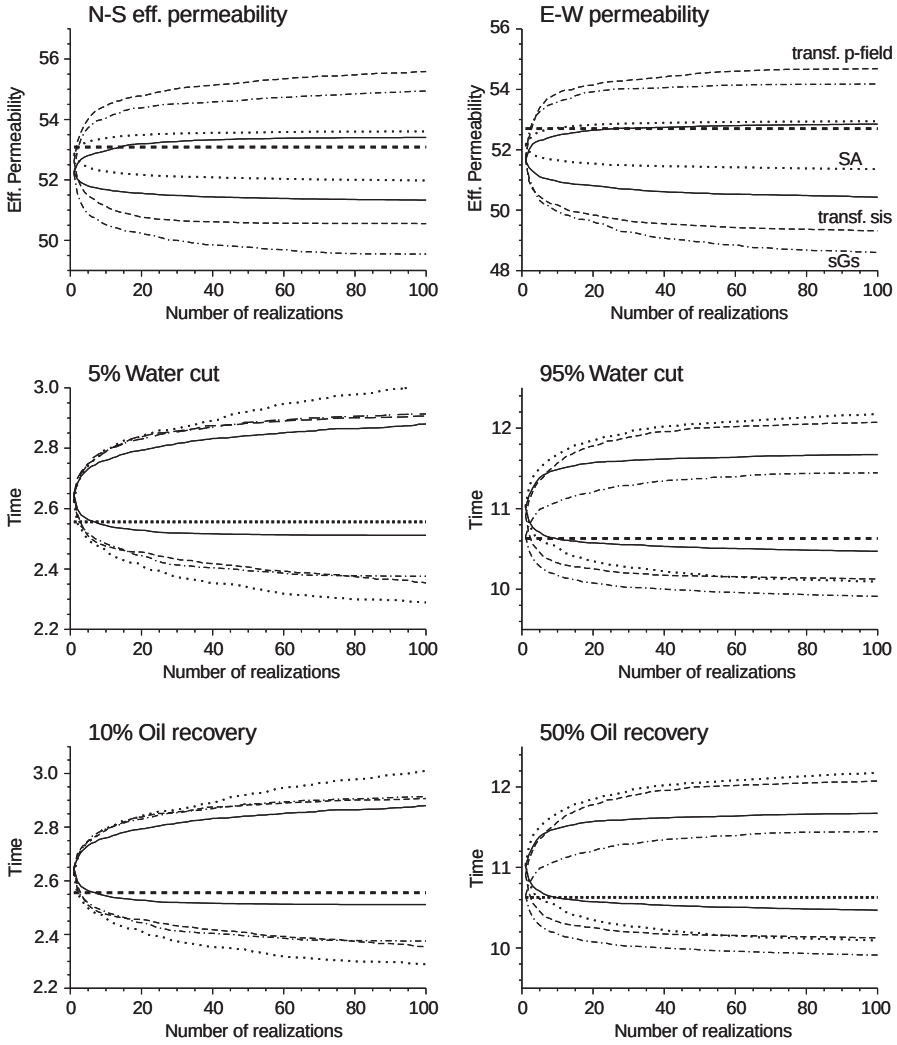

Fig. 10. Impact of the number of generated realizations on the upper and lower bounds of the space of uncertainty for the six flow properties. The horizontal dashed line denotes the true value derived from the reference image of Fig. 1. Best if the space is narrow and includes the true value. The algorithms are: — (transf. sis), - · - (sGs), - - (transf. *p*-field), · · · (SA)

Figure 9 (right column) indicates that the generation of 5 to 10 realizations allows one to improve the prediction of effective permeabilities, in particular for *p*-field simulation. For flow simulation results, differences between algorithms are more pronounced for long-term responses, that is 95% water cut. In other words, the intrinsic properties of permeability maps have an increasing impact as the flow simulation proceeds. For both water cut percentages, best results are obtained using sequential Gaussian simulation.

Figure 10 shows, for each simulation algorithm and response variable, the evolution of the upper and lower bounds of the space of uncertainty for increasing number of generated realizations. As expected, the extent of the space increases with the number of realizations, but at different rates depending on

the response variable and simulation algorithm. In this example, the increase generally becomes small beyond 20 realizations, although the convergence seems slower for short-term simulation results (5% water cut and 10% oil recovery), in particular for simulated annealing. With too few realizations, the space of uncertainty may not contain the true value depicted by the horizontal dashed line, e.g. less than 20 sis realizations for effective permeability. Regardless the response variable, *p*-field simulation yields the largest space with bounds similar to the ones generated by simulated annealing for flow simulation responses. For short-term responses, the sis space of uncertainty is included into the three other alike spaces. For long-term responses (95% water cut and 50% oil recovery), the sGs space gets smaller and centered on the true response value.

Conclusions

Although the conclusions that can be drawn from this study are, to some extent, specific to the Berea data set, it is clear that the space of uncertainty depicted by stochastic simulation may vary significantly from one algorithm to another, even when the same information (conditioning data, histogram, semivariogram) is being used. Differences between simulation algorithms are more pronounced for response variables that involve long runs of the flow simulator, such as the time to reach a 95% water cut. Prediction of reservoir performances thus do depend on the choice of the stochastic simulation algorithm, and it seems unlikely that the entire set of possible outcomes could be sampled by a single class of algorithm.

Reduction of ergodic fluctuations in the permeability histogram increases the precision (narrowness) of the response distribution generated by sequential indicator simulation and *p*-field simulation. There is also a substantial gain in accuracy because the sample histogram is here reasonably close to the reference histogram. Algorithms such as simulated annealing that imposes reproduction of the permeability histogram do not necessarily yield the narrowest distributions of response values. This is particularly true for flow simulation results because these are not controlled by a mere univariate distribution of permeability values. The swapping perturbation mechanism may be responsible for such variability in the results, and alternative mechanisms, such as the random sampling of local ccdfs, should be considered to achieve a better control of the local distributions of simulated values.

The extent of the space of uncertainty increases with the number of realizations generated. In this study, the rate of increase becomes small beyond 20 realizations; the convergence is slower for short-term simulation results (5% water cut and 10% oil recovery), in particular for simulated annealing. An algorithm might yield a probability distribution that is precise and accurate when many realizations are generated, but is inaccurate if derived from too few realizations. In many applications, stochastic simulation is used to identify "pessimistic" and "optimistic" scenarios, which means that the focus is on the edges of the space of uncertainty. The usual approach is to generate many realizations which are then processed through a transfer function, and the response values are used to rank realizations of attribute values from the most optimistic scenario to the most pessimistic one. It is important that extreme scenarios are encompassed in the response distribution, which is usually ensured by the computationally expensive generation of a large number of realizations. If only a few realizations can be afforded, one may prefer an algorithm such as *p*-field simulation that builds accurate and relatively precise distributions from small sets of realizations.

Response variables are generally correlated, hence the accuracy of each response distribution taken separately does not ensure the accuracy of the multivariate distribution of response values. Also, histograms of response variables should be supplemented by scattergrams to display bivariate relations betwen response variables, or more sophisticated multivariate statistical techniques (e.g., PCA) could be used to display multivariate spaces of uncertainty.

In this application, sequential Gaussian simulation yields both large goodness statistics and small local uncertainty, hence should be preferred for the generation of permeability maps. Sequential Gaussian simulation also provides the most precise and accurate spaces of uncertainty for long-term simulation results. It is still unclear why other algorithms that explicitly account for class-dependent patterns of spatial variability through indicator semivariograms do not perform better. Future studies should investigate the benefit of using more than 5 thresholds in the building of indicator-based ccdf models.

Although comparative studies are essentially descriptive and tied to a particular data set, they may point out problems related to the implementation of certain algorithms. For example, regardless the response variable, it appears that *p*-field simulation yields the largest space of uncertainty, even when ergodic fluctuations in the permeability histogram have been substantially reduced through a rank-preserving transform of simulated values. Current studies (Goovaerts, 1999) indicate that such a variability is mainly due to the non-conditioning of the probability field used to sample the local ccdfs, hence the present implementation of the algorithm should be modified. Similar remark applies to the perturbation mechanism in simulated annealing.

Another factor that influences the characteristics of the space of uncertainty and has not been addressed in this study is the sampling density. The number of conditioning data is here fairly large (5% sampling density), which tends to attenuate differences between algorithms. As this number decreases, one may expect an expansion of the spaces of uncertainty and largest differences between algorithms. Also, the sample histogram will be less reliable and imposing its reproduction by the set of simulated values should be less beneficial.

References

Christakos G (1992) Random Field Models in Earth Sciences: Academic Press, San Diego, p. 474

Davis JC (1986) Statistics and Data Analysis in Geology, 2nd Ed.: John Wiley & Sons, New York, p. 646

Deutsch CV (1994) Algorithmically-defined random function models, in Dimitrakopoulos R ed., Geostatistics for the Next Century: Kluwer Academic Publ., Dordrecht, p. 422–435

Deutsch CV (1997) Direct assessment of local accuracy and precision, in Baafi EY, Schofield NA, eds., Geostatistics Wollongong '96: Kluwer Academic Publ., Dordrecht, p. 115–125

Deutsch CV, Cockerham P (1994) Practical considerations in the application of simulated annealing to stochastic simulation: Math. Geology v. 26, no. 1, p. 67–82

Deutsch CV, Journel AG (1992) Annealing techniques applied to the integration of geological and engineering data: Stanford Center for Reservoir Forecasting, Stanford University, Unpublished annual report No 5

Deutsch CV, Journel AG (1998) GSLIB: Geostatistical Software Library and User's Guide, 2nd Ed.: Oxford University Press, New-York, p. 369

Deutsch CV, Wen X-H (1998). An improved perturbation mechanism for simulated annealing simulation: Math. Geology v. 30, no. 7, p. 801–816

ECLIPSE 100 Reference Manual, 1991, Intera ECL Petroleum Technologies, Highlands Farm, Greys Road, Henley-on-Thames, Oxfordshire, England

Farmer C (1988) The generation of stochastic fields of reservoir parameters with specified geostatistical distributions, in Edwards S, King P, eds., Mathematics in oil production: Clarendon Press, Oxford, p. 235–252
Froidevaux R (1993) Probability field simulation. in Soares A ed., Geostatistics Tróia '92, Quantitative geology and geostatistics: Kluwer Academic Publ., Dordrecht, p. 73–84.
Geman S, Geman D (1984) Stochastic relaxation, Gibbs distributions, and the Bayesian restoration of images: IEEE Trans. Pattern Anal. Machine Intell. PAMI, v. 6, n. 6, p. 721–741
Giordano R, Salter S, Mohanty K (1985) The effect of permeability variations on flow in porous media. SPE Paper Number 14365
Gómez-Hernández J (1997) Issues on environmental risk assessment. in Baafi EY, Schofield NA, eds., Geostatistics Wollongong '96: Kluwer Academic Publ., Dordrecht, p. 15–26
Gómez-Hernández J, Srivastava RM (1990) ISIM3D: An ANSI-C three-dimensional multiple indicator conditional simulation program: Computers & Geosciences, v. 16, p. 395–440
Gómez-Hernández J, Wen X (1994) To be or not to be multiGaussian? That is the question: Stanford Center for Reservoir Forecasting, Stanford University, Unpublished annual report No 7
Goovaerts P (1993) Spatial orthogonality of the principal components computed from coregionalized variables: Math. Geology, v. 25, no. 3, p. 281–302
Goovaerts P (1997) Geostatistics for Natural Resources Evaluation: Oxford University Press, New York, p. 483
Goovaerts P (1998a) Accounting for estimation optimality criteria in simulated annealing: Math. Geology, v. 30, no. 5, p. 511–534
Goovaerts P (1998b) Estimation or simulation of soil properties? An optimization problem with conflicting criteria: Geoderma, accepted
Goovaerts P (1999) p-field simulation using conditional probability fields, in preparation
Gotway CA, Rutherford BM (1994) Stochastic simulation for imaging spatial uncertainty: comparison and evaluation of available algorithms, in Armstrong M, Dowd PA, eds., Geostatistical Simulations, Kluwer Academic Publishers, Dordrecht, p. 1–21
Isaaks EH (1990) The Application of Monte Carlo Methods to the Analysis of Spatially Correlated Data, Doctoral dissertation, Stanford University, Stanford, CA
Journel AG (1994) The place of random functions in geostatistics: Geostatistics, v. 7, no. 2, p. 5–7
Journel AG (1997) The abuse of principles in model building and the quest for objectivity. in Baafi EY, Schofield NA, eds., Geostatistics Wollongong '96: Kluwer Academic Publ., Dordrecht, p. 3–14
Journel AG (1995) Probability fields: Another look and a proof: Stanford Center for Reservoir Forecasting, Stanford University, Unpublished annual report No 7
Journel AG, Alabert FG (1988) Focusing on spatial connectivity of extreme valued attributes: Stochastic indicator models of reservoir heterogeneities. SPE Paper Number 18324
Journel AG, Deutsch CV (1993) Entropy and spatial disorder: Math. Geology, v. 25, no. 3, p. 329–355
Journel AG, Xu W (1994) Posterior identification of histograms conditional to local data: Math. Geology, v. 26, no. 3, p. 323–359
Kaiser HF The varimax criterion for analytic rotation in factor analysis: Psychometrica, v. 23, p. 187–200
Myers DE (1994) Geostatistical simulation: thoughts and questions: Geostatistics, v. 7, no. 1, p. 4–7
Myers DE (1996) Choosing and using simulation algorithms, in Mowrer HT, Czaplewski RL, Hamre RH, eds., Spatial accuracy assessment in natural resources and environmental sciences: Second international symposium: General Technical Report RM-GTR-277: U.S. Department of Agriculture, Forest Service, Fort Collins, p. 23–29
Ripley BD (1981) Spatial Statistics: John Wiley & Sons, New York
Ripley BD (1987) Stochastic Simulation: John Wiley & Sons, New York, p. 237
Rossi RE (1994) Of tool makers and tool users: Geostatistics, v. 7, no. 2, p. 7–9
Srivastava RM (1992) Reservoir characterization with probability field simulation, in SPE Annual Conference and Exhibition, Washington, D.C., number 24753, Washington, D.C., Society of Petroleum Engineers, p. 927–938

Srivastava RM (1994) Thoughts and comments on conditional simulation algorithms: Geostatistics, v. 7, no. 2, p. 9–10
Srivastava RM (1996) An overview of stochastic spatial simulation, in Mowrer HT, Czaplewski, RL, Hamre RH, eds., Spatial accuracy assessment in natural resources and environmental sciences: Second international symposium: General Technical Report RM-GTR-277: U.S. Department of Agriculture, Forest Service, Fort Collins, p. 13–22
Srivastava RM (1997) Matheronian geostatistics: where is it going? in Baafi EY, Schofield NA, eds., Geostatistics Wollongong '96: Kluwer Academic Publ., Dordrecht, p. 55–66